Physicochemical Studies on Orientation and Conformation of a New Bacteriocin BacSp222 in a Planar Phospholipid Bilayer

Piotr Pieta,[†] Marta Majewska,[‡] ZhangFei Su[‡] Michael Grossutti,[‡] Benedykt Wladyka,[§] Marcin Piejko,[†] Jacek Lipkowski,[‡] Pawel Mak,[†]*

[†]Institute of Physical Chemistry Polish Academy of Sciences, Kasprzaka 44/52, 01-224 Warsaw, Poland

[‡]Department of Chemistry and [⊥]Department of Physics, University of Guelph, 50 Stone Road East, Guelph, Ontario, N1G 2W1, Canada

[§]Department of Analytical Biochemistry, Faculty of Biochemistry, Biophysics and Biotechnology, Jagiellonian University, Gronostajowa 7, 30-387 Krakow, Poland

[∥]3rd Department of General Surgery, Jagiellonian University Medical College, Pradnicka 35-37, 31-008 Krakow, Poland

ABSTRACT

The behavior, secondary structure, and orientation of a recently discovered bacteriocin-like peptide BacSp222 in a lipid model system supported at a gold electrode was investigated by chronocoulometry, polarization modulation infrared reflection absorption spectroscopy (PM-IRRAS) and attenuated total reflectance infrared (ATR-IR) spectroscopy. The IR spectra show that the secondary structure of BacSp222 is predominantly α-helical. Analysis of the spectra in the amide I region shows that the α-helical fragment of the peptide is inserted into bilayer at the potential range at which the bilayer is stable and attached to the Au(111) surface, i.e., from -0.5 to 0.3 V vs. Ag/AgCl. Insertion of BacSp222 to the membrane significantly changes the conformation of the acyl chains of lipid molecules, from all-trans to partially melted, however the chains become less tilted. Based on these results, we propose that BacSp222 interacts with the DMPC bilayer through the barrel-stave pore formation. In this model, α-helix of BacSp222 inserts into the membrane with an angle between the α–helix axis and membrane normal equal to ~18°. The changes in orientation of the α-helical fragment of the peptide indicate that the orientation of BacSp222 with respect to the bilayer surface is potential-dependent. The peptide is inserted into the membrane driven by the electrostatic field generated by negative charge at the metal surface. It is not inserted at negative potentials where the membrane is detached from the metal and no longer exposed to the electrostatic field of the metal.

INTRODUCTION

Antimicrobial peptides (AMPs) are promising candidates as potential alternatives for antibiotics, due to their unique properties such as amphipathicity, bioactivity, and non-specific interaction with bacteria cell membranes.[1] These small (6 to 100 amino acids) molecules play an important role in the innate immune system of almost all living organisms.[2] AMPs possess biocidal activities against Gram-negative and Gram-positive bacteria,[3] fungi,[4] viruses,[5] parasites,[6] and even tumor cells.[4, 5]

AMPs are considered for therapeutic use, drug delivery systems, bio-sensors and bacteria detection.[7] For instance, linear peptides based on the human cathelicidin LL-37 were utilized to promote skin wound healing,[8] cyclic peptides like MOG3 were employed in the treatment of multiple sclerosis in a mouse model,[9] melimine was immobilized onto contact lenses to provide antibacterial properties,[10] nanoparticles of poly(lactic-co-glycolic acid), PLGA, with encapsulated LL-37 were applied as a drug delivery system to promote wound healing.[11]

Natural AMPs are usually cationic with an average net charge of +4.6.[12] They usually interact with a cell membrane through non-specific mechanisms resulting in membranolytic activity.[13] Positively charged peptides interact with the negatively charged bacterial membranes mostly through electrostatic interactions. However, the mechanism of the membrane damage remains under debate. The mechanism of AMPs action depends on their properties, like secondary structure, amino-acid sequence, and in consequence amphipathicity. For instance magainin 2 (Mag 2), human LL-37, and alamethicin (Alm), disrupts bacterial membranes through the formation of toroidal (Mag 2 and LL-37) and barrel-stave pores (Alm).[14, 15, 16] Protegrin I, a β-hairpin AMP, acts by forming toroidal pores in lipid bilayers that mimic either the bacterial or the red blood cell membrane.[17] Dermaseptin and cecropin disintegrate the bacteria cell membrane

through the carpet-like model.[18, 19] Understanding the mechanism of AMPs action is of great importance for application of AMPs as a new kind of therapeutics. A variety of techniques have been utilized to study the interaction of AMPs with either artificial or natural cell membranes.[13]

BacSp222 is a recently discovered unique peptide, possessing features characteristic both for bacteriocins (the ability to kill bacteria) and virulence factors (toxicity toward host cells and the ability to modulate the host immune system activity).[20] The peptide is produced and excreted in high quantities by *Staphylococcus pseudintermedius* strain 222 isolated from dog skin lesions. The bacteriocin is a plasmid-encoded 50-amino acid long linear peptide, formylated on the N-terminus. BacSp222 is rich in tryptophan, lysine and arginine residues but its sequence dissimilar to all other known peptides or proteins. However, the biological activity, the size of the molecule, formylation, lack of cysteines, abundance in tryptophan and cationic residues makes it similar to a typical class II bacteriocins, which include aureocin A53,[21] epidermicin NI01,[22] and lacticin Q[23] as well as lacticin Z.[24] BacSp222 kills Gram-positive bacteria at MIC doses ranging from 0.1 to several μM and is inactive toward Gram-negative bacteria and fungi. In addition to bactericidal properties BacSp222 demonstrates significant activities toward eukaryotic cells. It is cytotoxic and also possesses immunomodulatory properties, efficiently enhancing IFNγ-induced NO release in murine macrophage-like cell lines.[20] BacSp222 was able to effectively release green fluorescent protein (GFP) from transformed bacterial cells indicating that the action of this peptide is related to massive disruption of cell membrane but, to date, nothing is known about the detailed mechanism of action of this bacteriocin. Moreover, immunomodulatory activities of BacSp222 suggest that it is able also to act on cells *via* specific protein receptor.

The objective of this study is to understand the mechanism of interaction of BacSp222 with a model biological membrane under electrochemical conditions. The ability to monitor the model

membrane with adsorbed peptides *in situ* under potential control allows for better mimic the electric field acting on a cell membrane.[25] In the present work chronocoulometry, PM-IRRAS, and ATR-IR measurements were performed to reveal the secondary structure of BacSp222 bound to the 1,2-dimyristoyl-sn-glycero-3-phosphocholine (DMPC) bilayer supported at a gold electrode surface. Although DMPC is not a good mimic of a bacterial membrane, this study sheds light on the interactions of BacSp222 with phospholipids. It is relevant for the design of the peptide delivery system and the understanding of its cytotoxic and immunomodulatory properties. The antimicrobial application depends on the balance between the amount of AMPs needed to kill the bacteria and amount causing cytotoxicity toward mammalian cell. Hence, it requires an understanding of the mechanism of the AMPs interaction with the membrane, such as that presented in this study.

DMPC is a suitable phospholipid for the PM-IRRAS measurements due its relatively low transition temperature (T_c) of 24 °C for DMPC and 21 °C for deuterated DMPC-d_{54}. This feature easily allows for experiments below T_c. Orientational and conformational changes to both the DMPC acyl chains and the α-helical part of BacSp222, induced by the applied potential, were monitored using these techniques. A significant result of this study is the demonstration that the insertion of BacSp222 is initiated by the penetration of its α-helical part into the bilayer. This result indicates that BacSp222 is able to form a pore in a biological membrane. In addition, this work provides unique information about the impact of the peptide insertion on the membrane structure. Another important result is the determination of the secondary structure of BacSp222.

EXPERIMENTAL SECTION

Chemicals

1,2-Dimyristoyl-*sn*-glycero-3-phosphocholine (DMPC) and 1,2-dimyristoyl-d_{54}-*sn*-glycero-3-phosphocholine (DMPC-d_{54}) were purchased from Avanti Polar Lipids. Potassium perchlorate (Bioultra, 99%) and deuterium oxide (D_2O, 99.99 atom % D) were from Sigma-Aldrich. All aqueous solutions were prepared with the use of ultrapure water (resistivity > 18.2 MΩ·cm) purified by a Milli-Q UV plus (Millipore) water system.

Bacteriocin BacSp222 was purified from *Staphylococcus pseudintermedius* 222 culture supernatant as described in detail elsewhere.[20] In brief, the deprived of bacteria post-culture medium was precipitated with ammonium sulphate, the precipitated material was redissolved and subjected to two steps of reverse-phase high pressure liquid chromatography (RP-HPLC) on a C18 and C8 columns, in turn. The fractions containing BacSp222 were collected, dried in a centrifugal evaporator, and stored at –20 °C until further use. The identity of the purified peptide was confirmed by mass spectrometry and Edman sequencing while the concentration of prepared solutions was determined by amino acid analysis as described previously.[26] The trifluoroacetic acid (TFA) was used during peptide purification. The TFA has IR band at 1673 cm^{-1} which may constitute a spectral interference for the analysis of the Amide I band of the peptide. The ATR spectra shown in Figure S5 demonstrated that the IR bands of TFA are very weak and that BacSp222 was effectively purified from TFA (Figure S5 and comments in the Supporting Information).

Sample Preparation

The vesicle fusion approach was utilized to deposit both DMPC and DMPC-d_{54}/BacSp222 (9:1 molar ratio) bilayer on the Au(111) surface. This approach was chosen because of BacSp222 is

soluble in water and due to limited amount of peptide we were unable to introduce it into the subphase of a Langmuir trough, in order to use the Langmuir-Blodgett and Langmuir-Schaefer approach to deposit the bilayer. Instead, Barenholz method was used to prepare small unilamellar vesicles (SUVs) of DMPC or DMPC-d_{54}.[27] In brief, a solution of DMPC in chloroform was added to a test tube. Next, chloroform was evaporated from the test tube using a stream of argon while the solution was being vortexed. After evaporation, the test tubes were stored in a desiccator under vacuum for at least 24 h prior to use. Then, a volume of ultrapure Milli-Q water or D_2O was added to dry lipid film such that a ~1 mg/mL suspension was obtained. The mixture was sonicated for 30 min at ~40 °C. To prepare DMPC-d_{54}/BacSp222 vesicles, an appropriate amount of 200 μg/mL solution of BacSp222 was added to the solution of DMPC-d_{54} vesicles and the solution was vortexed for 20 min. The DMPC bilayer was deposited by immersing the Au(111) electrode in the suspension of vesicles for 2 hrs. After vesicles deposition, the Au(111) electrode was removed from the solution and rinsed with ultrapure Milli-Q water.

For ATR-IR experiments, dry multibilayers of DMPC or DMPC-d_{54}/BacSp222 were deposited by drop-casting the vesicles dispersed in D_2O on a ZnSe internal reflection element. Then, D_2O was evaporated under a stream of nitrogen.

Chronocoulometry Measurements

The chronocoulometry measurements were carried out in an all-glass three-electrode cell with the hanging meniscus configuration using the procedure described elsewhere.[28] All measurements were performed at 18 °C. The cell was equipped with a single-crystal Au(111) working electrode (WE), which was grown, cut, and polished as described in the literature [29] and a gold wire counter electrode (CE), both of which were annealed using a hydrogen-oxygen flame and quenched with Milli-Q water to ensure that the surface was free from contamination. A

saturated calomel electrode (SCE) was used as the reference electrode (RE). The measurements were conducted with a HEKA PG 590 potentiostat/galvanostat and a lock-in amplifier (EG&G Instruments 7265 DSP). All data were acquired via a plug-in acquisition board (National Instruments NI-DAQ) using custom written software provided by Prof. Dan Brizzotto (University of British Columbia).

The RE used in the infrared cell was a Ag/AgCl electrode (with a potential of -42 mV with respect to the SCE electrode). Unless otherwise stated, all potentials are quoted with respect to the Ag/AgCl reference electrode.

Chronocoulometry was used to determine the charge density at the electrode surface by measuring the difference between the charge density at a potential E_i, where the bilayer lipid membrane is adsorbed onto the Au(111) surface, and at a potential E_{des}, where total desorption of the film takes place. First, the gold electrode was held at a base potential, E_b, of -0.1 V for 120s. The potential was then stepped to a variable potential of interest, E_i, where the electrode was held for 120 s. Next, the desorption potential, E_{des}, of -1.2 V was applied for 0.15 s and the current transient corresponding to desorption of the film and recharging of the interface was recorded. The integration of the current transients gives the difference between charge densities at potentials E_i and E_{des}.[30] This procedure was repeated two times for each point of the chronocoulometric curve with a freshly prepared bilayer. To determine the absolute charge of the bilayer, the same measurements were performed for the bare Au(111) electrode in the same supporting electrolyte. The absolute charge densities of bare Au(111) electrode were then calculated using the independent determined potential of zero charge (E_{pzc}) value of 0.215 V vs. Ag/AgCl.[31]

PM-IRRAS experiments

The PM-IRRAS experiments were performed using the procedure described previously.[29] The all glass spectroelectrochemical cell was equipped with a 1" CaF_2 equilateral prism (Janos Technology), a single-crystal Au(111) working electrode (WE), a Pt foil (Alfa Aesar, 99.99%) counter electrode, and a Ag/AgCl reference electrode. PM-IRRAS experiments were performed on a Nicolet Nexus 870 spectrometer (ThermoNicolet), equipped with an external tabletop optical mount (TOM) box, a mercury-cadmium-telluride (MCT-A) detector (TRS 50 MHz bandwidth, Nicolet), a photoelastic modulator (PEM) (Hinds Instruments PM-90 with a II/ZS50 ZnSe 50 kHz optical head), and a synchronous sampling demodulator (SSD) (GWC Instruments). Figure S1 of the Supporting Information shows a schematic of the PM-IRRAS set-up. The electrode potentials were controlled via a potentiostat (EG&G, PAR Model 362) using in-house software, an Omnic macro, and a digital-to-analog converter (Omega). In addition, Omnic Macro was used to collect and to save spectra. The CaF_2 prism was washed in water and methanol and then cleaned in an ozone UV chamber (UVO-cleaner, Jelight) for 20 min before being assembled in the cell. The electrode with assembled bilayer, was transferred to the cell, the cell was filled with 0.1 M $KClO_4$ solution, and argon (Linde) was gently bubbled for ~1 h to deaerate the solution. Then, the TOM box was purged for ~6 h prior to and throughout the entire experiment using CO_2 and H_2O-free air. First, the potential of the WE was set at -0.2 V vs. Ag/AgCl, and then spectra were acquired at a series of potentials, which were programmed as an increase of potential toward positive direction up to the potential of 0.3 V with 0.1 potential step. Then, the spectra were collected for potential starting from -0.3 V down to -0.8 V with -0.1 potential step. For each spectrum, 6000 scans were collected and averaged using an instrumental resolution of 4 cm^{-1}. This procedure was repeated two times with a freshly prepared bilayer.

When spectra are recorded with a resolution 4 cm^{-1} the data points are computed every 2 cm^{-1}. Since the bands are plotted by interpolation between these points the band centre position can be determined with uncertainty of 0.5 cm^{-1}.[32] All measurements were performed at 18 °C. PM-IRRAS measurements for each spectral region of interest were optimized by using an appropriate solvent, angle of incident, as well as electrolyte thickness between the IR prism and the electrode. The parameters used for spectra collection are listed in Table S1 of the Supporting Information.

ATR-IR Spectroscopy

To prepare multibilayer lipid films, vesicle suspension was deposited on a ZnSe-diamond ATR crystal under a stream of dry nitrogen gas. ATR-IR spectra were recorded on a Bruker Vertex 70 FTIR spectrometer equipped with an MCT-A detector and a zinc selenide wire-grid polarizer (Pike Technologies) using an incident angle of 45°. All measurements were performed at 18°C. The spectra were acquired at a resolution of 4 cm^{-1} as an average of 6000 scans. The ATR-IR spectra are expressed in absorbance units defined as $A = -\log(I/I_0)$, where I and I_0 are the infrared single beam intensities of the film and bare ATR crystal background, respectively. The absorbance spectra recorded for both p- and s-polarizations (A_p and A_s, respectively) were baseline-corrected, typically with a quadratic function, before further analysis. For quantitative calculations of molecular orientation, the following refractive indices were used: 2.44 for the ZnSe-diamond ATR crystal, 1.42 for DMPC acyl chains, and 1.00 for air.

Spectra Deconvolution and Peak Assignment

Combination of Fourier self-deconvolution (FSD), second derivative (SD), and generalized two-dimensional correlation spectroscopy (2D-COS)[33] were utilized to determine the number and position of peaks under the broad envelope of IR spectra. FSD (values of 17 cm^{-1} for the full

bandwidth at half maximum (fwhm) and 1.7 for the resolution enhancement factor were usually set) and SD (seven-data-point Savitzky-Golay algorithm was used) analysis were performed with the use of OMNIC v 6.0a (Thermo software). 2D-COS analysis was performed using the freeware 2DShigev v 1.3 (Shigeaki Morita). In our case, the external perturbation consisted of a variable potential applied to the electrode. The reference spectrum for all experiments was collected at 0.3 V vs. Ag/AgCl, which corresponds to the most positive potential of each set. From this analytical procedure, one obtains a synchronous and an asynchronous spectrum. We have used both components for peak determination. Once the number of peaks and their positions agree for the three independent determinations, FSD, SD, and 2D-COS, the peaks were assigned to their corresponding modes of vibration based on published literature.[29] Then, using PeakFit v 4.12 (Seasolve software), the spectral region was deconvoluted using mixed Lorentzian (DMPC-d_{54} spectra) or Gaussian (BacSp222 spectra) band shapes with an R^2 value of at least 0.99. The positions for all peaks were restricted to $\pm 2 cm^{-1}$ of the initial value determined from FSD, SD and/or 2D-COS, which is usually the variation between the values determined using the three procedures.

RESULTS AND DISCUSSION

1. Electrochemical behavior of the DMPC bilayer with incorporated BacSp222.

Before the PM-IRRAS study, both the DMPC and DMPC/BacSp222 bilayers supported on an Au(111) electrode were characterized using chronocoulometry. This technique was employed to determine the charge density at the electrode surface. The effect of peptide insertion into the DMPC bilayer on the potential-dependent properties of the bilayer and the potential range for which the bilayer is attached to the electrode surface were assessed. Figure 1 plots the charge density curves for the bare Au(111) electrode in a 0.1 M $KClO_4$ solution (curve 1) and for the

electrode with the DMPC (curve 2) and DMPC/BacSp222 bilayer (curve 3) deposited at Au(111). The bottom horizontal axis plots the potential applied to the Au(111) electrode vs. Ag/AgCl. The top horizontal axis plots the potential drop across the membrane (E - E_{pzc}) which is the equivalent to the transmembrane potential.[29]

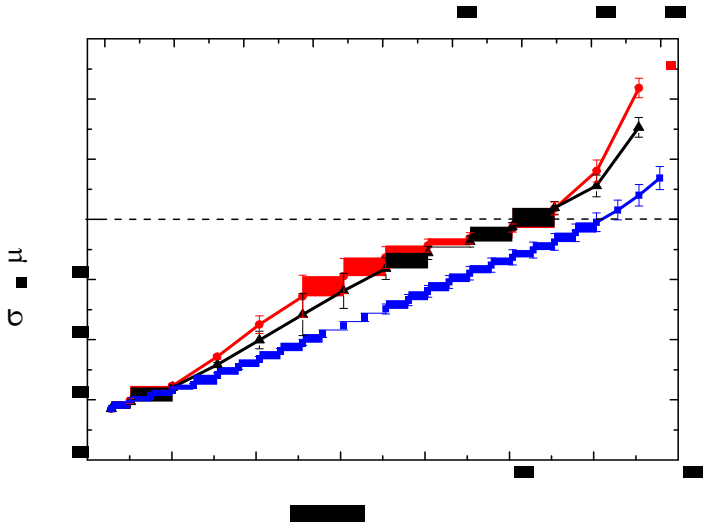

Figure 1. Charge density curves for a bare Au(111) electrode (curve 1) and the Au(111) electrode covered with the DMPC (curve 2) and DMPC/BacSp222 bilayer (curve 3) in a 0.1 M $KClO_4$ supporting electrolyte. The bottom horizontal axis plots the potential applied to the Au(111) electrode vs. Ag/AgCl. The top horizontal axis plots the potential drop across the membrane (E - E_{pzc}), which is an equivalent to the transmembrane potential.

The gold-electrolyte interface can be considered as a capacitor in which the gold surface can be charged by applying potential.[25] This charge on the metal surface is the physical variable associated with the electric field acting on the membrane. By applying potential in the range of -0.4 to 0.4 V vs. Ag/AgCl, at which the ~5 nm thick DMPC bilayer is adsorbed at the Au(111) electrode, the electric field acting on the bilayer is changed in the range of -1.0×10^8 to 2.0×10^7 V

m^{-1}.[34] These conditions mimic the transmembrane potential observed in a real biological cell membrane.[35] Figure 1 shows that by scanning the potential from zero charge (E_{pzc}) toward negative or positive direction, the gold-electrolyte interface is charged negatively or positively, respectively. The adsorption of both the DMPC and DMPC/BacSp222 bilayer decreases the charge stored at the gold-electrolyte interface. Consequently, the capacitance of the metal-electrolyte interface decreases upon organic molecules adsorption at the metal surface (when the metal is covered by a dielectric).[36] In the potential window from -0.7 to -0.2 V vs. Ag/AgCl (corresponding to transmembrane potentials between -0.75 and -0.15 V) less charge is stored by the interface when the electrode is covered by the DMPC/BacSp222 bilayer. This property indicates that this film has less defects or a thicker bilayer is formed in the presence of the peptide in the bilayer. PM-IRRAS experiments described in the next section will provide additional information concerning the impact of the peptide on the structure of the bilayer.

Moreover, a small ~0.16 V negative shift of E_{pzc} is observed after adsorption of the films on the electrode surface. The shift is due to the change of surface potential induced by oriented dipole moments which possess component in the direction normal to the electrode surface. This shift is comparable to the dipole potential measured in free standing phospholipid bilayers in vesicles[37]. The main contribution to the dipole potential is coming from differences in the hydration of the two leaflets of the bilayer[37]. In fact, neutron reflectivity[36] and ATR-IR measurements[38] demonstrated that the polar heads of lipids in contact with the metal are hydrated. The difference between hydration of the polar regions of the two leaflets of the gold supported bilayer may be seen as the origin of the measured dipole potential. Interestingly, there is no significant difference in the shift between the DMPC and DMPC/BacSp222 bilayers. Based on the amino acid sequence of BacSp222, it is a cationic peptide possessing positive charge.[20]

Insertion of positively charged BacSp222 into the DMPC bilayer would charge it positively. In that case the E_{pzc} should shift in the positive direction. The absence of the shift in the pzc between the DMPC and DMPC/BacSp222 bilayers indicates that BacSp222 does not possess a net charge at these conditions. It may also indicate that the factual isoelectric point (pI) of BacSp222 is equal to the pH of 0.1 M $KClO_4$ being 6.0.

The charge density curves recorded for the Au(111)/DMPC and Au(111)/DMPC/BacSp222 electrodes change slowly from -10 to 5 $\mu C\ cm^{-2}$ in the applied potential range from -0.3 to 0.2 V vs. Ag/AgCl corresponding to transmembrane potentials between -0.35 and -0.15 V. For more positive or more negative potentials, the change in the charge density curves is more rapid suggesting de-wetting of the bilayers.[39] Moreover, at potentials more negative than -0.7 V vs. Ag/AgCl (transmembrane potential is more negative than -0.75 V), the charge density curves corresponding to the electrodes covered with the bilayers (curves 2 and 3) merged with the curve for the bare Au(111) electrode (curve 1). It indicates that both the DMPC and DMPC/BacSp222 bilayers are detached from the metal surface. This behavior of the DMPC bilayer desorption was previously investigated by chronocoulometry,[40] elastic light scattering,[41] and neutron reflectivity measurements.[39] These studies showed that the DMPC bilayer is desorbed at negative potentials but remains in the close proximity, ~1 nm, to the electrode surface. The 1 nm gap between the Au(111) electrode and DMPC bilayer is filled with the solution. It was shown that the potential-induced changes of the charge density of the metal-solution interface are correlated with the orientational and conformational changes of the DMPC molecules.[30]

2. PM-IRRAS measurements of the DMPC and DMPC/BacSp222 bilayer.

2.1. Acyl Chain Region.

One of the most significant benefits of the PM-IRRAS measurements is the ability to determine changes in the conformation and orientation of molecules which are the building blocks of biological membranes.[35, 42] For membranes supported at a metal surface, these changes can be induced by an external electric field or interaction between components of the film.[43] In the present studies the tilt angle of the DMPC-d_{54} molecules in the presence of the BacSp222 molecules was determined by measuring IR spectra characteristic for the C−D stretching region (2000 and 2300 cm^{-1}). Deuterated DMPC (DMPC-d_{54}) was used to avoid spectral overlap with C-H stretching bands arising from BacSp222. Figure 2A shows the PM-IRRAS spectra of the C−D stretching region of DMPC-d_{54}, in the presence of BacSp222, centered at 2100 cm^{-1} recorded for the selected potentials applied to the Au(111) electrode as well as the calculated spectrum of randomly oriented molecules determined from optical constants (see details in the Supporting Information). Similar spectra recorded for DMPC-d_{54} without adsorbed BacSp222 are plotted in Figure S9 of the Supporting Information. Figure 2A shows that both the intensity and position of the bands change as a function of the applied potential.

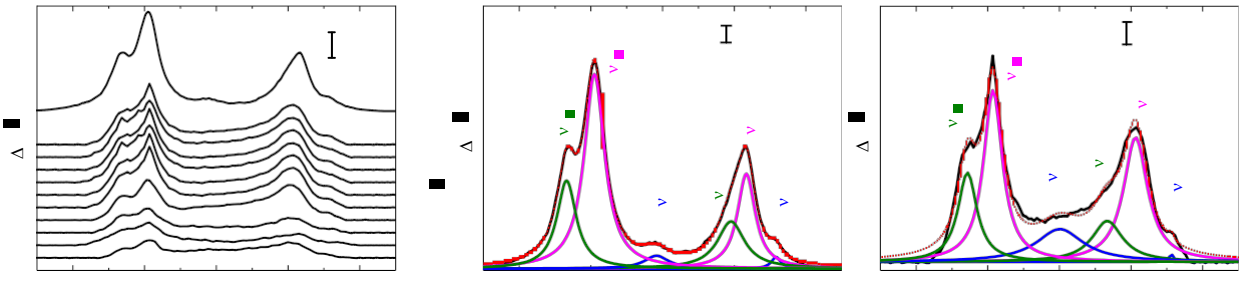

Figure 2. (A) C−D stretching region of PM-IRRAS spectra of the DMPC alkyl chains, in the presence of BacSp222 recorded at selected potentials vs. Ag/AgCl. The spectral deconvolution

(Lorentzian fit) of the calculated randomly oriented film and the experimental film measured at 0 V are shown in panels B and C, respectively.

Quantitative analysis of the PM-IRRAS spectra requires the deconvolution of the spectra into individual component bands (for details see Experimental Section). An example of the spectral deconvolution (Lorentzian fit) of the C−D stretching region is presented in Figures 2B and 2C for randomly oriented molecules calculated from the optical constants and the experimental data recorded at 0 V, respectively. The deconvolution of the spectra detected at selected potentials, for DMPC-d_{54} both in the presence and absence of BacSp222, are shown in the Supporting Information (Figs. S10 and S11, respectively). The deconvolution of the PM-IRRAS spectra allowed to localized the asymmetric, $\nu_{as}(CD_2)$, and symmetric, $\nu_s(CD_2)$, methylene stretching vibrations, located at ~2096 and ~2196 cm^{-1}, respectively.[44] Other bands corresponding to the CD_3 asymmetric, $\nu_{as}(CD_3)$, and symmetric, $\nu_s(CD_3)$, stretching observed at 2214 and 2115 cm^{-1}, respectively, were also deconvoluted. The two bands at ~2069 and ~2152 cm^{-1} correspond to the Fermi resonances of the bending modes of CD_3 and CD_2.[45] Both the position and intensity of these bands can be used for quantitative analysis of the bilayer in terms of the packing and conformation of the phospholipid tails within the membrane, as well as calculation of the average tilt angle of the acyl chains.[29]

Figure 3A shows the change of the $\nu_{as}(CD_2)$ and $\nu_s(CD_2)$ vibrations band as a function of potentials for DMPC-d_{54} both in the absence (curves *1* and *1*') and presence (curves *2* and *2*') of BacSp222. The position of $\nu_{as}(CD_2)$ does not change significantly within the entire potential window either in the absence or in the presence of BacSp222 (curves *1* and *2*, respectively). The average values of these positions are equal to ~2196 cm^{-1}. For an all-trans conformation, the positions of the $\nu_{as}(CD_2)$ is ~2191 cm^{-1}.[43] The blue shift of the band position suggests that the

acyl chains of DMPC-d_{54} are partially melted and contain gauche conformations. The position of the $\nu_s(CD_2)$ band for the DMPC-d_{54} in the absence of BacSp222 (curve *1'*) is also constant and equal to ~2092 cm^{-1} for the potential range between -0.4 and 0.3 V. For all-trans conformation the frequency of this band is expected to be 2088 cm^{-1}.[43] Therefore, the position of the $\nu_s(CD_2)$ band also indicates that the chains are partially melted. Then, for potentials more negative than -0.4 V, a shift of ~4 cm^{-1} towards higher frequency is observed. The blue shift of the $\nu_s(CD_2)$ band position suggests that a further melting of the acyl chains (increase in the density of gauche conformations in the chains) occurs at these negative potentials. These changes in the $\nu_s(CD_2)$ band position are accompanied by the broadening of the band. Such changes are characteristic of hydrocarbon chain-melting observed at the gel to liquid-crystalline phase transition of hydrated phospholipid bilayers.[46] The $\nu_s(CD_2)$ band position for DMPC-d_{54} in the presence of BacSp222 (curve *2'*) is constant for the entire potential window. Its average value equals to 2096 cm^{-1} and is approximately equal to the band position in the absence of BacSp222 (curve *1'*), at potentials more negative than -0.4 V. It indicates that the interaction of the peptide with the hydrophobic core of the lipid membrane leads to an increase in disorder of the acyl chains.[47] Similar behavior was observed for gramicidin A, Alm, and bacteriorhodopsin upon interaction with a DMPC bilayer.[43] Above T_c of DMPC and at higher concentration these peptides caused an increase in the lipid chain gauche conformers. The PM-IRRAS results correspond very well with the chronocoulometric measurements which showed that the presence of BacSp222 leads to a decrease of the capacitance of the interface (smaller slope of charge density vs. potential (curve 3 in Figure 1) at E>-0.4 V). A liquid crystalline-like bilayer, in which the lipid molecules are more mobile, is expected to have less defects and hence to form more compact film.

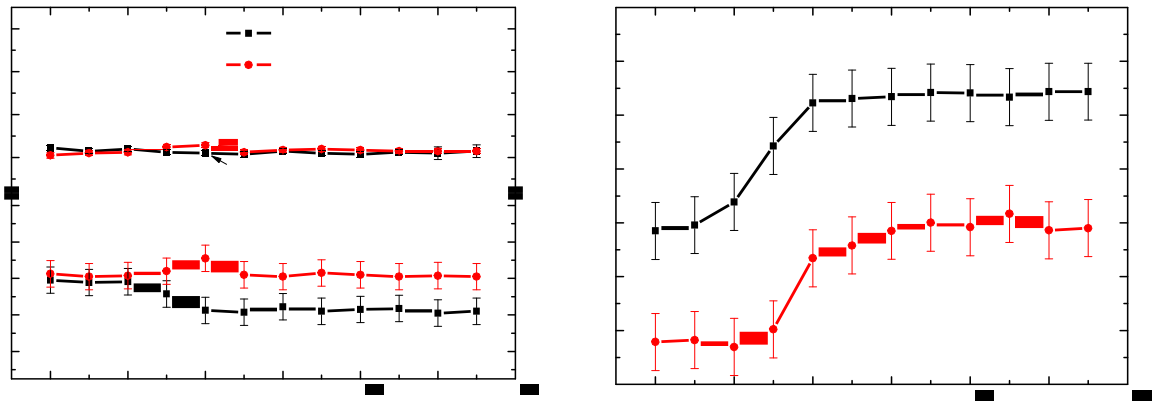

Figure 3. (A) Peak positions of the $\nu_{as}(CD_2)$ and $\nu_s(CD_2)$ bands in the absence (curves 1 and 1') and in the presence (curves 2 and 2') of BacSp222; (B) The tilt angle of the trans fragment of the DMPC alkyl chains plotted as a function of the applied potential for a DMPC bilayer in the absence (curve 1) and presence (curve 2) of BacSp222.

Quantitative analysis of the orientation of the DMPC-d_{54} in the absence and presence of BacSp222 in a membrane were performed by calculating the tilt angle of the acyl chains of the DMPC-d_{54} molecules (Θ_{DMPC}), using the procedure described elsewhere.[39] Details concerning the calculations are described in the Supporting Information.

Figure 3B shows the dependence of the average tilt angle of the trans fragments of acyl chains of DMPC-d_{54} on the applied potential both in the absence (curve *1*) and presence (curve *2*) of BacSp222. It should be emphasized that acyl chains receive gauche conformations and are not fully stretched as it is in case of trans conformation. That is why one can only determine the average angle between the direction normal to the plane of the CH_2 moieties and surface normal which corresponds to the average tilt of trans fragments of the chains. This number is used as a measure of the tilt of the chains. There is no significant change in the tilt angle of acyl chains in the potential range from 0.3 to -0.4 V vs Ag/AgCl. This behavior indicates that electrostriction

has little effect on the orientation of the lipid molecules. This conclusion is consistent with detailed discussion of the impact of electrostriction on the orientation of lipids in the metal supported bilayer, given elsewhere.[34] Its value is approximately equal to 37° and 23° in the absence and presence of BacSp222, respectively. The average tilt angle is much lower in the presence of BacSp222. Clearly, adsorption of BacSp222 significantly changes not only conformation but also orientation of the DMPC-d_{54} molecules. After adsorption of BacSp222 the acyl chains of DMPC-d_{54} are less tilted. As expected,[34] for potentials less negative then -0.6 V the tilt angle decreases for both films but still it is lower for the DMPC-d_{54}/BacSp222 bilayer.

2.2. Amide Stretching Region of BacSp222

The amide I band is the most valuable vibration band of the protein backbone providing information about the protein secondary structure.[48-49] This band originates from the C=O stretching vibration of the amide group (~80%)[48-49] and gives rise to IR bands in the region from ~1700 to ~1600 cm^{-1}. For complex peptides which consist of a variety of structural elements such like α-helices, β-sheets, β-turns, and non-ordered structures the amide I band is composed of sub-bands, which have characteristic frequencies. These bands overlap forming a complex amide I band envelope. The resulting amide I band is broad and its analysis requires deconvolution.[49] Figure 4 shows the PM-IRRAS spectra for the amide I band of BacSp222 incorporated into the DMPC-d_{54} bilayer measured at various potentials and for a randomly oriented BacSp222. The spectrum for a randomly oriented BacSp222 was calculated from optical constants (Figure S3 of the Supporting Information). Since DMPC-d_{54} molecules do not absorb IR photons between 1600 to 1700 cm^{-1} region,[42] the IR band in Figure 4 originates from BacSp222 present in the bilayer.

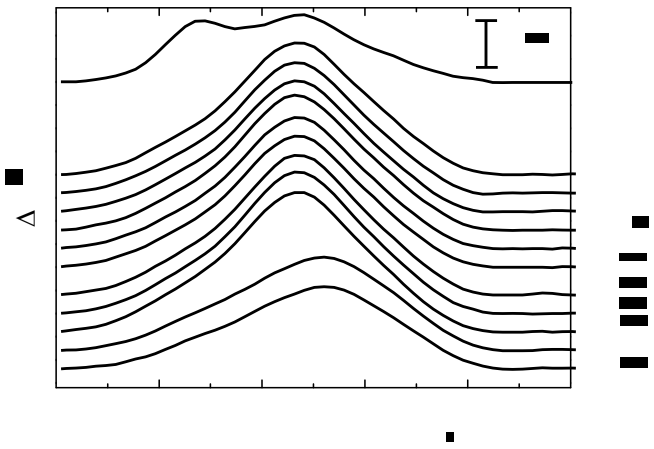

Figure 4. PM-IRRAS spectra for the amide I band of the BacSp222 for selected potentials versus Ag/AgCl.

The intensity of the amide I bands recorded for the selected potentials are much higher than that for the calculated spectrum. In the random DMPC-d_{54}/BacSp222 film, two peaks at ~1654 and ~1673 cm^{-1} are clearly visible. The position of these peaks are characteristic for α-helical and β-turn secondary structures, respectively. These structures are dominant in the IR spectrum of BacSP222 molecules. In the spectra measured for BacSp222 in the bilayer supported at a gold electrode, the peak at 1673 cm^{-1} is much weaker. The α-helix is the most pronounced structural component contributing to the IR spectra of BacSp222. In the PM-IRRAS spectra, the band intensity does not change significantly in the potentials region from 0.3 to -0.5 V vs. Ag/AgCl. However, a significant change is observed for more negative potentials than -0.6 V vs. Ag/AgCl. At these negative potentials the DMPC-d_{54}/BacSp222 film is detached from the surface of Au(111) (curve 3 in Figure 1). The band intensity dramatically decreases for spectra recorded at -0.7 and -0.8 V (Figure 4). It suggests that both orientational and conformational changes occur at this potential range. These changes can be visualized with the help of two-dimensional correlation spectroscopy (2D-COS), described in details in the Supporting Information.[50]

The 2D correlation spectroscopy revealed that at least three bands at ~1641, ~1655, and ~1674 cm^{-1} can be identified in the broad envelope of the Amide I spectrum (Figure S4 of the Supporting Information). The position of the component bands were additionally confirmed by performing both SD and FSD of the spectra. Then, the positions of the individual bands obtained from 2D-COS, SD and FSD were used for the deconvolution of the amide I band. The SD and FSD data processing revealed that sub-bands centered at ~1635, ~1654, and ~1674 cm^{-1} can be identified for randomly oriented BacSp222 (Figure S12 of the Supporting Information). The amide I band of randomly oriented BacSp222 was deconvoluted using a Gaussian fit assuming that the three bands are present in the region (Figure 5A). The band at ~1635 cm^{-1} corresponds to the β-sheet structure.[51] The two dominant bands centered at 1654 and 1674 cm^{-1} can be assigned to the α-helical and β-turns structures, respectively.[51, 52, 53, 54, 55] The fwhm was 22.5, 16.9, and 15.9 cm^{-1} for bands centered at 1654, 1634, and 1674 cm^{-1}, respectively. Assuming that the absolute value of the transition dipole of the amide I band has the same value for different secondary structures,[55] the integrated band intensity can be used to estimate that the BacSp222 molecule is predominantly α-helical (58%) but β-turn (32%) and β-sheet (10%) secondary structures are also present.

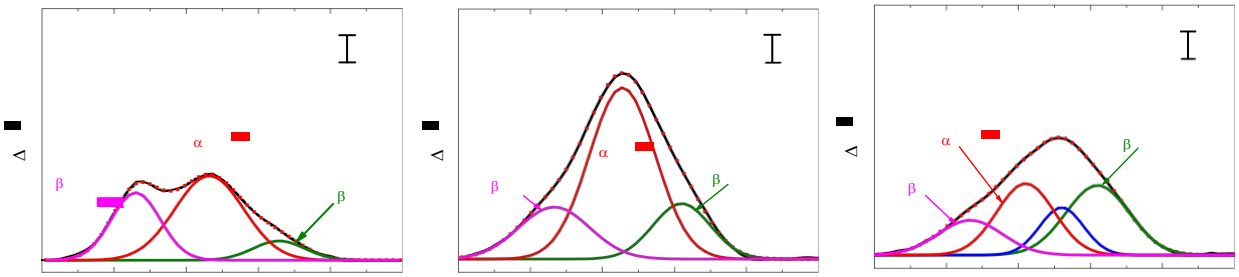

Figure 5. Deconvolution of the amide I band of BacSp222 (A) random film and incorporated in the DMPC bilayer recorded at the potential of (B) 0.1 and (C) -0.8 V.

A similar deconvolution procedure was performed for the amide I band for the PM-IRRAS spectra of the DMPC-d_{54}/BacSp222 film recorded at the selected potentials (depicted in Figure S12 of the Supporting Information). Figure 5B and 5C show deconvolution of the amide I band recorded at the potentials 0.1 and -0.8 V vs. Ag/AgCl, respectively. Those spectra were chosen to show changes in the amide I band of BacSp222 caused by the change of the applied potential. Three sub-bands were fitted to the experimental data with the help of the SD and FSD data analysis. The spectra recorded for a potential range from 0.2 to -0.5 V vs. Ag/AgCl did not change significantly. The band at ~1654 cm^{-1} is dominant with the fwhm between 21 and 23 cm^{-1}. The two other bands at ~1635 (fwhm ~19 cm^{-1}) and ~1678 cm^{-1} (fwhm ~22 cm^{-1}) are much smaller than the band at ~1654 cm^{-1}. Importantly, positions of bands determined by using FSD and SD correspond very well with bands determined by using 2D correlation spectroscopy. The decrease of potential to -0.8 V vs. Ag/AgCl leads to significant changes in the structure of the amide I band. That is, the intensity of the α-helix band decreases in favor of a new band at ~1649 cm^{-1} (fwhm ~14 cm^{-1}). The new band at 1649 cm^{-1} can be assigned to the random structure[48], suggesting that potential smaller than -0.6 V induces slow unfolding of the BacSp222 molecules.

The α-helical part of the peptide is mainly responsible for insertion into the DMPC bilayer. Therefore it was chosen to determine the possible orientation of BacSp222 in the phospholipid bilayer. The band arising from the α-helix secondary structure was used to calculate the angles between the transition dipole moment of the α-helical part of BacSp222 and electrode surface normal, Θ , (Eq. S5 of the Supporting Information). Figure 6A shows the calculated angles of the transition dipole as a function of applied potential. The tilt angle of the transition dipole moment

of the α-helix of BacSp222 is potential independent between -0.5 to 0.3 V and equal to 39º (Figure 6A and Table S2 of the Supporting Information). But for the potentials at which the bilayer is detached from the electrode surface the angle increases to the value of 61º. This clearly indicates that the potential changes induce orientational changes in the helical part of the BacSp222 secondary structure. Using the calculated angle between the transition dipole moment and surface normal, the average tilt angle of the helices, γ, with the respect to the surface normal was calculated (Eq. S7 of the Supporting Information). The angle between the α-helix long axis and the transition moment of the amide I vibration (reference angle), α , was determined to be between 34° and 38°[56, 57, 58, 59]. The tilt angle of the α-helix was calculated according to the procedure described elsewhere [60] and details of these calculations are given in the Supporting Information.

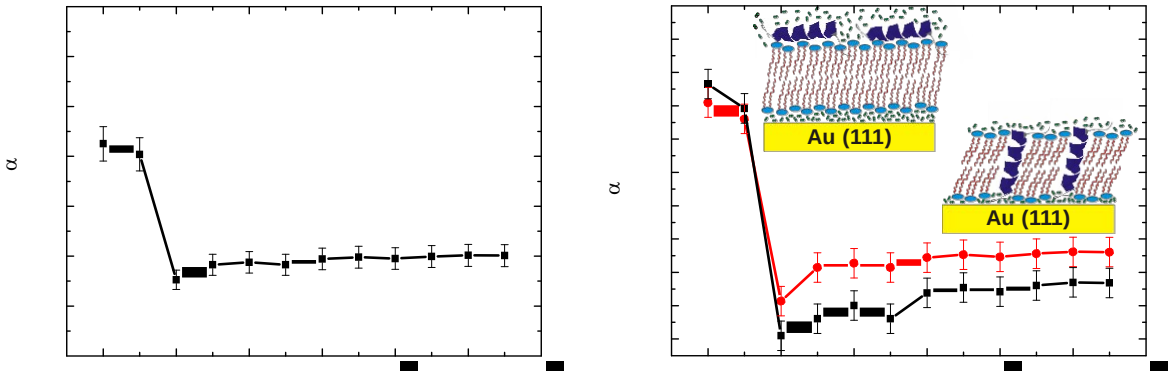

Figure 6. Tilt angle of (A) the transition dipole moments and (B) the major axis of the α-helix component of BacSp222 as a function of the electrode potential vs. Ag/AgCl. The tilt angle of the α-helix was calculated for reference angle of 34º (●) and 38º (■). The cartoons show how the

lipids and BacSp222 molecules are arranged on the electrode surface when the bilayer is adsorbed and desorbed from the electrode.

Figure 6B plots tilt angles of the α-helical part of BacSp222 as a function of the applied potential calculated for two reference angles of 34° and 38°. For potentials at which the film is stable and attached to the Au(111) surface, i.e., from -0.5 to 0.3 V, the α-helix is inserted into the bilayer. The average tilt angle for this potential window is equal to either 24° or 12° depending on the value of the reference angle (either 34° or 38°) used in the calculations, respectively. These values are characteristic for the inserted state. But at potentials more negative than -0.6 V the orientation of the α-helix changes to 70-75° with respect to the normal to the surface which can be considered as the surface state.

These results provide direct evidence that the BacSp222 molecule interacts with the DMPC-d_{54} bilayer by inserting α-helices into the membrane when it is exposed to the static electric field provided by the charge on the metal. It is significant to note that the peptide is not inserted when the bilayer is detached from the metal at the negative end of potentials where it is floating in the vicinity of the metal surface on a ~1 nm thick cushion of electrolyte. At that state the electrostatic field is not acting on the bilayer. This behavior indicates that the insertion is field-driven and the peptide may discriminate between negatively charged bacterial cell bilayers and bilayers made of zwitterionic phospholipids present in mammalian cells. This behavior is characteristic for peptides which form pores in the phospholipid bilayer.[13] It was shown that lacticin Q, which is similar to BacSp222, forms pores in a negatively charged phospholipid bilayer described by the toroidal model.[61] In the toroidal model the lipid molecules undergo significant reorientation to form the pore leading to an increase of the tilt of their lipid chains. In our studies, the tilt angles

of the acyl chains decreases in the presence of BacSp222 (Figure 3B). This result excludes a possibility of the toroidal pore formation and indicates that the barrel-stave model may be applied in the present case.

We have also performed ATR-FTIR studies of BacSp222 in a dry DMPC multibilayer-film. These experiments are described in the Supporting Information. The order parameters for the acyl chains and the α-helix determined from these experiments (Table S3) show that the order of the lipid chains in the multibilayer film is not affected by the presence of BacSp222, however, the secondary structure of BacSp222 is changed. The amide I band shows presence of α-helix, β-turns, and β-sheets structures. However, the percentage of the α-helix structure to the overall band intensity is lower than in the hydrated state investigated by PM-IRRAS. The calculated tilt angle of the α-helical part of BacSp222, with respect to the surface normal, for dry multibilayer film is equal to 62°. This number indicates that the peptide is in the surface state. These results suggest that the hydration level of the bilayer has a significant influence on the orientation of the BacSp222 molecules.

Conclusions

In conclusion, this work shows how a new bacteriocin-like peptide named BacSp222 interacts with DMPC bilayers. The structural composition of adsorbed BacSp222 is predominately α-helical (58%), but other components like β-turns (32%) and β-sheets (10%), are also present. Similar values have been obtained for the secondary structure of BacSp222 determined in solution using CD.[20] This strongly suggests that the peptide is intrinsically ordered and its conformation does not change significantly upon adsorption to the membrane. Interestingly, the

majority of α-helical antimicrobial peptides generally do not have ordered structures in solution, and only fold gradually to form helices upon interaction with membranes.[62]

PM-IRRAS results show that adsorption of BacSp222 significantly changes not only the conformation of the DMPC molecules, from predominantly trans to partially melted, but also their orientation. The DMPC acyl chains are less tilted after insertion of BacSp222. The potential applied to the electrode induce orientational changes of the helical part of the secondary structure of BacSp222. Moreover, at potentials lower than E = -0.6 V slow unfolding of the BacSp222 molecules occurs. At potentials higher than E = -0.6 V, the BacSp222 molecule is stable and its α-helical part inserts into the DMPC bilayer. Inserted state of the BacSp222 molecules may indicate that these peptides interact with a biological membrane via barrel-stave pore formation. The combination of PM-IRRAS and ATR-IR experiments shows that hydration level of the DMPC bilayer strongly affects the secondary structure and orientation of BacSp222 in the membrane. That is, for dry multibilayer system, the peptides are in the surface state with respect to the plane of the membrane.

ASSOCIATED CONTENT

Supporting Information

Details of experimental procedures and methods are presented. Table S1 contains a summary of the conditions used to obtain the PMIRRAS spectral regions for the various functional groups of the DMPC-d_{54}/BacSp222. Table S2 contains values of order parameters and corresponding angles of transition dipole moments, Θ, and α-helix long axes, γ , vs applied potential. Table S3 lists the lipid acyl chain order parameters and corresponding tilt angles for DMPC multibilayers

in the absence and presence of BacSp222. Figure S1 shows the experimental PM-IRRAS set-up. Figures S2 and S3 correspond to the optical constants for the C-D stretching region of the phospholipid bilayer and the amide I band of BacSp222. Figure S4 depicts synchronous and asynchronous 2D correlation spectra of the amide I band of BacSp222 recorded at selected potentials. Figure S5 shows ATR-IR spectra with wavenumbers characteristic for TFA. Figures S6-S8 show the ATR-FTIR spectra of BacSp222 in a dry DMPC multibilayer-film. Figure S9 shows the PM-IRRAS spectra for the C−D stretching region of the DMPC-d_{54} alkyl chains in the absence of BacSp222 for selected potentials vs. Ag/AgCl and the spectral deconvolution of the calculated randomly oriented film and the experimental film measured at 0 V. Figures S10 and S11 show deconvolution of the C−D stretching bands of DMPC-d_{54} in the presence and absence of BacSp222. Figure S12 shows deconvolution of the amide I band of BacSp222 together with the Fourier Self-deconvolution and second derivative data processing. This material is available free of charge via the Internet at http://pubs.acs.org.

AUTHOR INFORMATION

Corresponding Authors

*E-mail: ppieta@ichf.edu.pl Fax: +48 (22) 343 33 33

jlipkowski@uoguelph.ca Fax: +01 519-766-1499

pawel.mak@uj.edu.pl Fax: +48 (12) 664 69 15

Author Contributions

P.P., ZF.S., P.M., and J.L. planned the experiments. P.P, M.M, ZF.S, P.M, B.W., M.P., and M.G performed the experiments. All authors analyzed the data. P.P., P.M., and J.L wrote the manuscript. All authors reviewed the manuscript.

Notes

The authors declare no competing financial interest.

ACKNOWLEDGMENTS

The study was supported in parts by the grant HOMING PLUS/2012-6/11 (to PP) from the Foundation for Polish Science (Warszawa, Poland), by Discovery grant from the National Sciences and Engineering Research Council of Canada (to JL), and by the grant UMO-2013/11/B/NZ6/00409 (to PM) from the National Science Center (Krakow, Poland). The Faculty of Biochemistry, Biophysics and Biotechnology of Jagiellonian University is a partner of the Leading National Research Center (KNOW) supported by the Ministry of Science and Higher Education, Warsaw, Poland. The research was partially carried out using equipment purchased through European Union structural funds (project "Malopolska Centre of Biotechnology" No POIG.02.01.00-12-167/08).

REFERENCES

1. Nguyen, L. T.; Haney, E. F.; Vogel, H. J. The Expanding Scope of Antimicrobial Peptide Structures and Their Modes of Action. *Trends Biotechnol.* **2011,** *29*, 464-472.

2. Hancock, R. E. Cationic Peptides: Effectors in Innate Immunity and Novel Antimicrobials. *Lancet Infect. Dis.* **2001,** *1*, 156-64.

3. Mor, A.; Nicolas, P. Isolation and Structure of Novel Defensive Peptides from Frog Skin. *Eur. J. Biochem.* **1994,** *219*, 145-154.

4. Rozek, T.; Wegener, K. L.; Bowie, J. H.; Olver, I. N.; Carver, J. A.; Wallace, J. C.; Tyler, M. J. The Antibiotic and Anticancer Active Aurein Peptides from the Australian Bell Frogs

Litoria aurea and *Litoria raniformis.* The Solution Structure of Aurein 1.2. *Eur. J. Biochem.* **2000,** *267*, 5330-5341.

5. Chernysh, S.; Kim, S. I.; Bekker, G.; Pleskach, V. A.; Filatova, N. A.; Anikin, V. B.; Platonov, V. G.; Bulet, P. Antiviral and Antitumor Peptides From Insects. *Proc. Natl. Acad. Sci. U. S. A.* **2002,** *99*, 12628-12632.

6. Simmaco, M.; Mignogna, G.; Canofeni, S.; Miele, R.; Mangoni, M. L.; Barra, D. Temporins, Antimicrobial Peptides from the European Red Frog *Rana Temporaria*. *Eur. J. Biochem.* **1996,** *242*, 788-792.

7. Wang, G.; Mishra, B.; Lau, K.; Lushnikova, T.; Golla, R.; Wang, X. Antimicrobial Peptides in 2014. *Pharmaceuticals (Basel)* **2015,** *8*, 123-50.

8. Woo, J. I.; Kil, S. H.; Brough, D. E.; Lee, Y. J.; Lim, D. J.; Moon, S. K. Therapeutic Potential of Adenovirus-Mediated Delivery of β-Defensin 2 for Experimental Otitis Media. *Innate Immun.* **2015,** *21*, 215-224.

9. Wang, C. K.; Gruber, C. W.; Cemazar, M.; Siatskas, C.; Tagore, P.; Payne, N.; Sun, G. Z.; Wang, S. H.; Bernard, C. C.; Craik, D. J. Molecular Grafting onto a Stable Framework Yields Novel Cyclic Peptides for the Treatment of Multiple Sclerosis. *ACS Chem. Biol.* **2014,** *9*, 156-163.

10. Dutta, D.; Ozkan, J.; Willcox, M. D. P. Biocompatibility of Antimicrobial Melimine Lenses: Rabbit and Human Studies. *Optometry Vision Sci.* **2014,** *91*, 570-581.

11. Chereddy, K. K.; Her, C. H.; Comune, M.; Moia, C.; Lopes, A.; Porporato, P. E.; Vanacker, J.; Lam, M. C.; Steinstraesser, L.; Sonveaux, P.; Zhu, H. J.; Ferreira, L. S.; Vandermeulen, G.; Preat, V. PLGA Nanoparticles Loaded with Host Defense Peptide LL37 Promote Wound Healing. *J. Controlled Release* **2014,** *194*, 138-147.

12. Wang, Z.; Wang, G. APD: The Antimicrobial Peptide Database. *Nucleic Acids Res.* **2004,** *32*, D590-2.

13. Brogden, K. A. Antimicrobial Peptides: Pore Formers or Metabolic Inhibitors in Bacteria? *Nat. Rev. Microbiol.* **2005,** *3*, 238-250.

14. Fox, R. O.; Richards, F. M. A Voltage-Gated Ion Channel Model Inferred from the Crystal Structure of Alamethicin at 1.5-Å Resolution. *Nature* **1982,** *300*, 325-330.

15. Lee, C. C.; Sun, Y.; Qian, S.; Huang, H. W. Transmembrane Pores Formed by Human Antimicrobial Peptide LL-37. *Biophys. J.* **2011,** *100*, 1688-1696.

16. Tamba, Y.; Ariyama, H.; Levadny, V.; Yamazaki, M. Kinetic Pathway of Antimicrobial Peptide Magainin 2-Induced Pore Formation in Lipid Membranes. *J. Phys. Chem. B* **2010,** *114*, 12018-12026.

17. Mani, R.; Cady, S. D.; Tang, M.; Waring, A. J.; Lehrert, R. I.; Hong, M. Membrane-Dependent Oligomeric Structure and Pore Formation of β-Hairpin Antimicrobial Peptide in Lipid Bilayers from Solid-State NMR. *Proc. Natl. Acad. Sci. U. S. A.* **2006,** *103*, 16242-16247.

18. Bechinger, B.; Lohner, K. Detergent-like Actions of Linear Amphipathic Cationic Antimicrobial Peptides. *Biochim. Biophys. Acta-Biomembr.* **2006,** *1758*, 1529-1539.

19. Gazit, E.; Boman, A.; Boman, H. G.; Shai, Y. Interaction of the Mammalian Antibacterial Peptide Cecropin P1 with Phospholipid Vesicles. *Biochemistry-Us* **1995,** *34*, 11479-11488.

20. Wladyka, B.; Piejko, M.; Bzowska, M.; Pieta, P.; Krzysik, M.; Mazurek, L.; Guevara-Lora, I.; Bukowski, M.; Sabat, A. J.; Friedrich, A. W.; Bonar, E.; Miedzobrodzki, J.; Dubin, A.; Mak, P. A Peptide Factor Secreted by *Staphylococcus pseudintermedius* Exhibits Properties of both Bacteriocins and Virulence Factors. *Sci. Rep.* **2015,** *5*, 14569.

21. Netz, D. J. A.; Pohl, R.; Beck-Sickinger, A. G.; Selmer, T.; Pierik, A. J.; Bastos, M. D. D.; Sahl, H. G. Biochemical Characterisation and Genetic Analysis of Aureocin A53, a New, Atypical Bacteriocin from *Staphylococcus aureus*. *J. Mol. Biol.* **2002,** *319*, 745-756.

22. Sandiford, S.; Upton, M. Identification, Characterization, and Recombinant Expression of Epidermicin NI01, a Novel Unmodified Bacteriocin Produced by *Staphylococcus epidermidis* that Displays Potent Activity Against *Staphylococci*. *Antimicrob. Agents Chemother.* **2012,** *56*, 1539-1547.

23. Fujita, K.; Ichimasa, S.; Zendo, T.; Koga, S.; Yoneyama, F.; Nakayama, J.; Sonomoto, K. Structural Analysis and Characterization of Lacticin Q, a Novel Bacteriocin Belonging to a New Family of Unmodified Bacteriocins of Gram-Positive Bacteria. *Appl. Environ. Microb.* **2007,** *73*, 2871-2877.

24. Iwatani, S.; Zendo, T.; Yoneyama, F.; Nakayama, J.; Sonomoto, K. Characterization and Structure Analysis of a Novel Bacteriocin, Lacticin Z, Produced by *Lactococcus lactis* QU 14. *Biosci. Biotech. Bioch.* **2007,** *71*, 1984-1992.

25. Lipkowski, J. Building Biomimetic Membrane at a Gold Electrode Surface. *Phys. Chem. Chem. Phys.* **2010,** *12*, 13874-13887.

26. Wladyka, B.; Wielebska, K.; Wloka, M.; Bochenska, O.; Dubin, G.; Dubin, A.; Mak, P. Isolation, Biochemical Characterization, and Cloning of a Bacteriocin from the Poultry-Associated *Staphylococcus aureus* strain CH-91. *Appl. Microbiol. Biotechnol.* **2013,** *97*, 7229-7239.

27. Barenholz, Y.; Gibbes, D.; Litman, B. J.; Goll, J.; Thompson, T. E.; Carlson, F. D. Simple Method for Preparation of Homogeneous Phospholipid Vesicles. *Biochemistry-Us* **1977,** *16*, 2806-2810.

28. Lipkowski, J. Biomimetic Membrane Supported at a Metal Electrode Surface. A Molecular View. In *Advances in Planar Lipid Bilayers and Liposomes* Iglic, A.; Kulkarni, C. V., Eds.; Academic Press: Burlington, 2014; Vol. 20, pp 1-49.

29. Kycia, A. H.; Su, Z. F.; Brosseau, C. L.; Lipkowski, J. In Situ PM–IRRAS Studies of Biomimetic Membranes Supported at Gold Electrode Surfaces In *Vibrational Spectroscopy at Electrified Interfaces*, Wieckowski, A.; Korzeniewski, C.; Braunschweig, B., Eds.; John Wiley & Sons: Hoboken, 2013, p 345.

30. Zawisza, I.; Lachenwitzer, A.; Zamlynny, V.; Horswell, S. L.; Goddard, J. D.; Lipkowski, J. Electrochemical and Photon Polarization Modulation Infrared Reflection Absorption Spectroscopy Study of the Electric Field Driven Transformations of a Phospholipid Bilayer Supported at a Gold Electrode Surface. *Biophys. J.* **2003,** *85*, 4055-4075.

31. Laredo, T.; Leitch, J.; Chen, M. H.; Burgess, I. J.; Dutcher, J. R.; Lipkowski, J. Measurement of the Charge Number Per Adsorbed Molecule and Packing Densities of Self-Assembled Long-Chain Monolayers of Thiols. *Langmuir* **2007,** *23*, 6205-6211.

32. Griffith, P. R.; de Haseth, J. E. *Fourier Transform Infrared Spectrometry*; John Wiley and Sons: New York, 1986.

33. Noda, I.; Dowrey, A. E.; Marcott, C.; Story, G. M.; Ozaki, Y. Generalized Two-Dimensional Correlation Spectroscopy. *Appl. Spectrosc.* **2000,** *54*, 236a-248a.

34. Zawisza, I.; Bin, X. M.; Lipkowski, J. Potential-driven structural changes in Langmuir-Blodgett DMPC bilayers determined by in situ spectroelectrochemical PM IRRAS. *Langmuir* **2007,** *23*, 5180-5194.

35. Brand, I. Application of Infrared Spectroscopy for Structural Analysis of Planar Lipid Bilayers under Electrochemical Control. *Adv. Planar Lipid Bilayers Liposomes* **2013,** *18*, 21-62.

36. Damaskin, B. B.; Petrii, O. A.; Batrakov, V. V. *Adsorption of Organic Compounds on Electrodes*; Plenum Press: New York, 1971.

37. Gross, E.; Bedlack, R. S.; Loew, L. M. Dual-Wavelength Ratiometric Fluorescence Measurement of the Membrane Dipole Potential. *Biophys. J.* **1994,** *67*, 208-216.

38. Uchida, T.; Osawa, M.; Lipkowski, J. SEIRAS studies of water structure at the gold electrode surface in the presence of supported lipid bilayer. *J. Electroanal. Chem.* **2014,** *716*, 112-119.

39. Burgess, I.; Li, M.; Horswell, S. L.; Szymanski, G.; Lipkowski, J.; Majewski, J.; Satija, S. Electric Field-Driven Transformations of a Supported Model Biological Membrane - An Electrochemical and Neutron Reflectivity Study. *Biophys. J.* **2004,** *86*, 1763-1776.

40. Horswell, S. L.; Zamlynny, V.; Li, H. Q.; Merrill, A. R.; Lipkowski, J. Electrochemical and PM-IRRAS Studies of Potential Controlled Transformations of Phospholipid Layers on Au(111) Electrodes. *Faraday Discuss.* **2002,** *121*, 405-422.

41. Bizzotto, D.; Zamlynny, V.; Burgess, I.; Jeffrey, C. A.; Li, H. Q.; Rubinstein, J.; Galus, Z.; Nelson, A.; Pettinger, B.; Merrill, A. R.; Lipkowski, J. Amphiphilic and Ionic Surfactants at Electrode Surfaces. In *Interfacial Electrochemistry, Theory, Experiment and Applications.*, A. Wieckowski, M. D., Ed.: New York, 1999, pp 405-426.

42. Zamlynny, V.; Lipkowski, J. Quantitative SNIFTIRS and PM IRRAS of Organic Molecules at Electrode Surface. In *Diffraction and Spectroscopic Methods in Electrochemistry*, Alkire, R. C.; Kolb, D. M.; Lipkowski, J.; Ross, P. N., Eds.; WILEY-VCH Verlag GmbH & Co. KGaA Weinheim, 2006; Vol. 9, pp p. 315-376.

43. Lee, D. C.; Durrani, A. A.; Chapman, D. A Difference Infrared Spectroscopic Study of Gramicidin A, Alamethicin, and Bacteriorhodopsin in Perdeuterated Dimyristoylphosphatidylcholine. *Biochim. Biophys. Acta* **1984,** *769*, 49-56.

44. Brosseau, C. L.; Leitch, J.; Bin, X.; Chen, M.; Roscoe, S. G.; Lipkowski, J. Electrochemical and PM-IRRAS a Glycolipid-Containing Biomimetic Membrane Prepared Using Langmuir-Blodgett/Langmuir-Schaefer Deposition. *Langmuir* **2008,** *24*, 13058-13067.

45. Liang, C. Y.; Lytton, M. R. Infrared Spectra of Crystalline and Stereoregular Polymers. *J. Polym. Sci.* **1962,** *61*, S45-S48.

46. Pare, C.; Lafleur, M.; Liu, F.; Lewis, R. N. A. H.; McElhaney, R. N. Differential Scanning Calorimetry and H-2 Nuclear Magnetic Resonance and Fourier Transform Infrared Spectroscopy Studies of the Effects of Transmembrane Ex-Helical Peptides on the Organization of Phosphatidylcholine Bilayers. *Biochim. Biophys. Acta-Biomembr.* **2001,** *1511*, 60-73.

47. Sikorska, E.; Ilowska, E.; Wyrzykowski, D.; Kwiatkowska, A. Membrane Structure and Interactions of Peptide Hormones with Model Lipid Bilayers. *Biochim. Biophys. Acta-Biomembr.* **2012,** *1818*, 2982-2993.

48. Kong, J.; Yu, S. Fourier Transform Infrared Spectroscopic Analysis of Protein Secondary Structures. *Acta Biochim. Biophys. Sinica* **2007,** *39*, 549-559.

49. Surewicz, W. K.; Mantsch, H. H.; Chapman, D. Determination of Protein Secondary Structure by Fourier Transform Infrared Spectroscopy: A Critical Assessment. *Biochemistry-Us* **1993,** *32*, 389-394.

50. Noda, I.; Ozaki, Y. *Two-Dimensional Correlation Spectroscopy: Applications in Vibrational and Optical Spectroscopy*; John Wiley & Sons Ltd.: Chichester, West Sussex, England, 2004.

51. Byler, D. M.; Susi, H. Examination of the Secondary Structure of Proteins by Deconvolved FTIR Spectra. *Biopolymers* **1986,** *25*, 469-487.

52. Goormaghtigh, E.; Ruysschaert, J. M.; Raussens, V. Evaluation of the Information Content in Infrared Spectra for Protein Secondary Structure Determination. *Biophys. J.* **2006,** *90*, 2946-2957.

53. Goormaghtigh, E.; Vigneron, L.; Knibiehler, M.; Lazdunski, C.; Ruysschaert, J. M. Secondary Structure of the Membrane-Bound Form of the Pore-Forming Domain of Colicin A. An Attenuated Total-Reflection Polarized Fourier-Transform Infrared Spectroscopy Study. *Eur. J. Biochem.* **1991,** *202*, 1299-1305.

54. Goormaghtigh, E.; Demeutter, J.; Szoka, F.; Cabiaux, V.; Parente, R. A.; Ruysschaert, J. M. Secondary Structure and Orientation of the Amphipathic Peptide GALA in Lipid Structures. An Infrared-Spectroscopic Approach. *Eur. J. Biochem.* **1991,** *195*, 421-429.

55. Surewicz, W. K.; Mantsch, H. H. New Insight into Protein Secondary Structure from Resolution-Enhanced Infrared Spectra. *Biochim. Biophys. Acta* **1988,** *952*, 115-130.

56. Miyazawa, T.; Blout, E. R. The Infrared Spectra of Polypeptides in Various Conformations: Amide I and II Bands. *J. Am. Chem. Soc.* **1961,** *83*, 712-719.

57. Marsh, D.; Muller, M.; Schmitt, F. J. Orientation of the Infrared Transition Moments for an Alpha-Helix. *Biophys. J.* **2000,** *78*, 2499-2510.

58. Okamura, E.; Umemura, J.; Takenaka, T. Molecular Orientation in Thin Langmuir-Blodgett Films of Dipalmitoylphosphatidylcholine as Studies by FTIR Transmission and Reflection-Absorption Spectroscopy. *Can. J. Chem.* **1991,** *69*, 1691-1694.

59. Tsuboi, M. Infrared Dichroism and Molecular Conformation of α-Form Poly-γ-Benzyl-L-Glutamate. *J. Polym. Sci.* **1962,** *59*, 139-153.

60. Leitch, J. J.; Brosseau, C. L.; Roscoe, S. G.; Bessonov, K.; Dutcher, J. R.; Lipkowski, J. Electrochemical and PM-IRRAS Characterization of Cholera Toxin Binding at a Model Biological Membrane. *Langmuir* **2013,** *29*, 965-976.

61. Yoneyama, F.; Imura, Y.; Ohno, K.; Zendo, T.; Nakayama, J.; Matsuzaki, K.; Sonomoto, K. Peptide-Lipid Huge Toroidal Pore, a New Antimicrobial Mechanism Mediated by a Lactococcal Bacteriocin, Lacticin Q. *Antimicrob. Agents Chemother.* **2009,** *53*, 3211-3217.

62. Mak, P.; Szewczyk, A.; Mickowska, B.; Kicinska, A.; Dubin, A. Effect of Antimicrobial Apomyoglobin 56-131 Peptide on Liposomes and Planar Lipid Bilayer Membrane. *Int. J. Antimicrob. Agents* **2001,** *17*, 137-142.

Table of Contents